THE MFS FOR THE IDENTIFICATION OF A SOUND-SOFT INTERIOR ACOUSTIC SCATTERER

A. KARAGEORGHIS, D. LESNIC, AND L. MARIN

Abstract. We employ the method of fundamental solutions (MFS) for detecting a sound-soft scatterer surrounding a host acoustic homogeneous medium due to a given point source inside it. The measurements are taken inside the medium and, in addition, are contaminated with noise. The MFS discretization yields a nonlinear constrained regularized minimization problem which is solved using standard software. The results of several numerical experiments are presented and discussed.

1. INTRODUCTION

In this paper we consider the inverse problem of determining the boundary of a sound-soft acoustic scatterer from noisy internal measurements generated by an internal point source. This inverse mathematical formulation models the determination of the extent of a reservoir from the data obtained by lowering a transmitter-receiver combination through a bore hole into the reservoir [23]. This interior problem is apparently more difficult than the usually addressed exterior scattering problem because all the scattered waves are now trapped inside the domain and are repeatedly reflected off its boundary [23, 22], see, also, [24]. In addition, this problem is still nonlinear and ill-posed and therefore difficult to solve. In particular, in [23] the determination of the boundary of a sound-soft scatterer was achieved using the linear sampling method while the same method was used for the recovery of an impedance boundary in [24]. In [12], the structural integrity of a cavity was tested using the Kirsch-Kress approach applied to the analytical extension of the scattered field to the interior of the tested domain via the solution of the corresponding Cauchy problem. The boundary of the scatterer in [22] was obtained using a regularized Newton iterative approach. It should be noted that the representation of the solution as a single-layer potential with sources distributed inside the scatterer has previously been used by Kirsch and Kress [16, 17].

The method of fundamental solution (MFS) is a meshless Trefftz method which has, in recent years, been extensively used for the numerical solution of inverse geometric problems [14]. More specifically, it has been frequently used for inverse geometric problems in acoustics, see e.g. [18, 20, 25]. In contrast to the boundary integral equation method which has also been used for the solution of obstacle scattering problems [11, 13], the MFS requires neither the meshing of the

boundary nor surface integration and is thus considerably easier to implement. In it, the solution is approximated by a linear combination of fundamental solutions of the Helmholtz operator with singularities placed on a pseudo-boundary surrounding the solution domain [7].

The method proposed in this work is similar to the method proposed in [1] in which, however, the inverse problem considered is different as it is the exterior boundary that is unknown, and the measurements are taken on an internal boundary. This type of approach has also been considered in [3] although the inverse scatterers were not considered to encircle the measurement boundary.

The paper is organized as follows. The mathematical formulations of the direct and inverse problems are presented in Section 2. The MFS is described in Section 3. Numerical results are presented and discussed in Section 4 and, finally, some concluding remarks and ideas for future work are provided in Section 5.

2. MATHEMATICAL FORMULATION

Physically, we consider the interior scattering with a wave number $k > 0$ due to a given point source $\boldsymbol{z}_0$ inside the two-dimensional, bounded and simply-connected scatterer domain D with a C^2 boundary ∂D. This means that the incident field is given by

$$u^{\mathrm{inc}}(\boldsymbol{x}) = \Phi(\boldsymbol{x}, \boldsymbol{z}_0) := \frac{\mathrm{i}}{4} H_0^{(1)}(k|\boldsymbol{x} - \boldsymbol{z}_0|), \quad \boldsymbol{x} \in \mathbb{R}^2, \tag{2.1}$$

where i is the imaginary unit and $H_0^{(1)}$ denotes the Hankel function of first kind and of order zero. The scattered field u^{s} satisfies the Helmholtz equation

$$\Delta u^{\mathrm{s}} + k^2 u^{\mathrm{s}} = 0 \quad \text{in} \quad D. \tag{2.2}$$

For impenetrable scatterers the boundary condition on ∂D is of the form

$$\mathcal{B}(u) = 0 \quad \text{on} \quad \partial D, \tag{2.3}$$

where $u = u^{\mathrm{inc}} + u^{\mathrm{s}}$ represents the total field and the boundary operator $\mathcal{B}$ models the physical properties of the scatterer, e.g.

$$\mathcal{B}(u) = u, \quad \text{sound soft}, \tag{2.4a}$$

$$\mathcal{B}(u) = \frac{\partial u}{\partial \nu}, \quad \text{sound hard}, \quad \text{where } \boldsymbol{\nu} \text{ is the outward unit normal vector to } \partial D, \tag{2.4b}$$

$$\mathcal{B}(u) = \begin{cases} u \quad \text{on} \quad \partial D_1, \\ \\ \dfrac{\partial u}{\partial \nu} \quad \text{on} \quad \partial D_2, \end{cases} \quad \text{mixed}, \quad \text{where } \partial D_1 \cup \partial D_2 = \partial D, \tag{2.4c}$$

$$\mathcal{B}(u) = \lambda u + \frac{\partial u}{\partial \nu}, \quad \text{impedance}, \quad \text{where } \lambda \text{ is the reciprocal of the impedance.} \tag{2.4d}$$

We assume that:
(A) k^2 is not an eigenvalue of $-\Delta$ in D with respect to the boundary condition (2.3).

2.1. **The direct problem.** Under assumption (A), it is well-known, see e.g. [5], that the direct scattering problem which requires finding u^s satisfying (2.2) and (2.3), when D is known, is well-posed.

In the sequel, we consider the sound-soft scatterer in which case the Dirichlet boundary condition recasts as

$$u^s(\boldsymbol{x}) + \frac{\mathrm{i}}{4} H_0^{(1)}(k|\boldsymbol{x} - \boldsymbol{z}_0|) = 0, \quad \boldsymbol{x} \in \partial D. \tag{2.5}$$

2.2. **The inverse problem.** We consider the Helmholtz equation (2.2) subject to the Dirichlet boundary condition (2.5) but now the boundary ∂D is unknown and has to be determined from additional measurements of u^s on some known interior closed curve Γ assumed to lie inside D. The condition that $\boldsymbol{z}_0 \in \Gamma$ is not essential but in what follows we shall assume, for simplicity, that Γ is the circle of radius $|\boldsymbol{z}_0| > 0$ centred at the origin, i.e.

$$\Gamma = \partial B_{|\boldsymbol{z}_0|}(\boldsymbol{0}). \tag{2.6}$$

Then the above additional condition is

$$u^s(\boldsymbol{x}) = f(\boldsymbol{x}), \quad \boldsymbol{x} \in \Gamma, \tag{2.7}$$

where f is some given measured data which may be contaminated with noise. Of course, for compatible data, the function f in (2.7) depends on $\boldsymbol{z}_0$.

Assuming that:

(B) k^2 is not a Dirichlet eigenvalue of $-\Delta$ in the interior of Γ,

then the boundary ∂D is uniquely determined from the knowledge of the (matrix) scattered field (2.7) for all $\boldsymbol{x}$ and $\boldsymbol{z}_0$ on Γ, see [23]. Note that assumption (B) is not essential since we can always re-shape and re-scale the given curve Γ, see [26]. The above uniqueness result requires knowledge of the scattered field $u^s(\boldsymbol{x}; \boldsymbol{z}_0)$ for all $\boldsymbol{x}, \boldsymbol{z}_0 \in \Gamma$, hence for infinitely many point sources $\boldsymbol{z}_0 \in \Gamma$. However, under the usual assumption, see [6]:

(C) D is contained in a disk of radius t_0/k, where $t_0 = 2.40482$ is the first positive root of the Bessel function J_0,

the boundary ∂D can be uniquely determined from only one measurement (2.7) for the scattered field u^s at a single point source $\boldsymbol{z}_0 \in \Gamma$, see [22]. Note that this assumption limits the diameter of D to the tested wave numbers k in the sense that for higher wave numbers, the diameter of D must be small enough.

The geometry of the problem in depicted in Figure 1.

3. THE METHOD OF FUNDAMENTAL SOLUTIONS (MFS)

In the MFS we seek the solution of the inverse Helmholtz problem (2.2), (2.5) and (2.7) in the form, see e.g. [7],

$$u_M^s(\boldsymbol{x}) = \sum_{m=1}^{M} c_m \, G(\boldsymbol{x}, \boldsymbol{y}_m), \qquad \boldsymbol{x} \in \overline{D}, \tag{3.1}$$
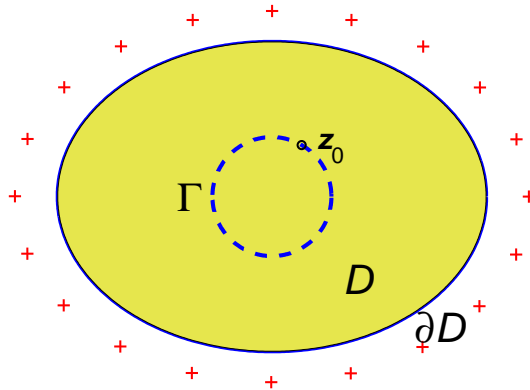
FIGURE 1. Geometry of the problem. The crosses $+$ denote the MFS singularities.

where $\boldsymbol{y}_m \in \mathbb{R}^2 \backslash \overline{D}$ are singularities, as shown in Figure 1, and $c_m \in \mathbb{C}$ are unknown complex coefficients to be determined by imposing boundary condition (2.5) and condition (2.7). Moreover, G is the fundamental solution of the two-dimensional Helmholtz operator given by [7]

$$G(\boldsymbol{x}, \boldsymbol{y}) = \frac{\mathrm{i}}{4} H_0^{(1)}(k|\boldsymbol{x} - \boldsymbol{y}|). \tag{3.2}$$

We assume that the unknown boundary ∂D is a smooth, star-like curve with respect to the origin. This means that its equation in polar coordinates can be written as

$$x = r(\vartheta) \cos \vartheta, \qquad y = r(\vartheta) \sin \vartheta, \qquad \vartheta \in [0, 2\pi), \tag{3.3}$$

where r is a smooth $2\pi-$periodic function.

If we let $\vartheta_m = 2\pi(m-1)/M$ for $m = \overline{1, M}$, be a uniform discretization of the interval $[0, 2\pi)$, then the discretized form of (3.3) for ∂D becomes

$$r_m = r(\vartheta_m), \quad m = \overline{1, M}. \tag{3.4}$$

On the unknown star-shaped boundary ∂D we consider the points

$$\boldsymbol{x}_m = r_m \left(\cos \vartheta_m, \, \sin \vartheta_m \right), \qquad m = \overline{1, M}, \tag{3.5}$$

expressed in polar coordinates, where the radii $r_m > 0$ are unknown. The MFS singularities are taken to be

$$\boldsymbol{y}_m = \eta \, r_m \left(\cos \vartheta_m, \, \sin \vartheta_m \right), \qquad m = \overline{1, M}, \tag{3.6}$$

where $\eta > 1$ is an unknown magnification parameter to be determined as part of the solution, see the description of the moving pseudo-boundary MFS in [15]. Moreover, the measured data (2.7)

are given at the points on the circle Γ, see (2.6),

$$\tilde{\boldsymbol{x}}_\ell = |\boldsymbol{z}_0| \, (\cos \varphi_\ell, \, \sin \varphi_\ell) \,, \quad \varphi_\ell = 2\pi(\ell - 1)/L, \quad \ell = \overline{1, L}. \tag{3.7}$$

We thus have $3M + 1$ unknowns, namely the radii $\boldsymbol{r} = (r_m)_{m=\overline{1,M}}$, the complex coefficients $\boldsymbol{c} = (c_m)_{m=\overline{1,M}}$ and the magnification parameter η in (3.6). These are determined by imposing the (complex) boundary condition (2.1) at the M points $(\boldsymbol{x}_m)_{m=1}^M$ which yield $2M$ equations, and by imposing the (complex) condition (2.7) at the L points $(\tilde{\boldsymbol{x}}_\ell)_{\ell=1}^L$ which yield an additional $2L$ equations. We thus have $2M + 2L$ equations in $3M + 1$ unknowns and therefore need to take $2L \geq M + 1$.

To obtain a stable approximation to the inverse problem, we minimize the regularized nonlinear least-squares functional

$$T_{\lambda_1,\lambda_2}(\boldsymbol{c}, \boldsymbol{r}, \eta) := \sum_{m=1}^M \left| \sum_{j=1}^M c_j \, G(\boldsymbol{x}_m, \boldsymbol{y}_j) + \frac{\mathrm{i}}{4} H_0^{(1)}(k|\boldsymbol{x}_m - \boldsymbol{z}_0|) \right|^2$$

$$+ \sum_{\ell=1}^L \left| \sum_{j=1}^M c_j \, G(\tilde{\boldsymbol{x}}_\ell, \boldsymbol{y}_j) - f^\varepsilon(\tilde{\boldsymbol{x}}_\ell) \right|^2 + \lambda_1 \sum_{j=1}^M |c_j|^2 + \lambda_2 \sum_{m=2}^M (r_m - r_{m-1})^2, \tag{3.8}$$

where $\lambda_1, \lambda_2 \geq 0$ are regularization parameters, subject to the simple bounds on the variables

$$|\boldsymbol{z}_0| < r_m < \zeta_2 = 2.40482/k, \quad m = \overline{1, M}, \quad \text{and} \quad 1 < \eta < 2. \tag{3.9}$$

The data (2.7) come from practical measurements which are inherently contaminated with errors due to noise, and we therefore replace f by f^ε, and in computation, the noisy data are generated as

$$f^\varepsilon(\tilde{\boldsymbol{x}}_\ell) = (1 + \rho_\ell \, p) \, f(\tilde{\boldsymbol{x}}_\ell), \quad \ell = \overline{1, L}, \tag{3.10}$$

where p represents the percentage of noise added to the data (2.7) on Γ, and ρ_ℓ is a pseudo-random noisy variable drawn from a uniform distribution in $[-1, 1]$ using the MATLAB$^©$ [21] command `-1+2*rand(1,L)`.

The first sum in (3.8) corresponds to the satisfaction of the boundary condition (2.5), whereas the second sum corresponds to the perturbed internal measurement condition (3.10). Since the inverse problem is ill-posed, in (3.8), the regularization terms $\lambda_1 \sum_{j=1}^M |c_j|^2$ and $\lambda_2 \sum_{m=2}^M (r_m - r_{m-1})^2$ are added in order to achieve the stability of the numerical MFS solution u_M and of the smooth boundary ∂D.

The above constrained optimization problem (3.8) and (3.9) is solved using the MATLAB$^©$ toolbox routine `lsqnonlin` which does not require supplying the gradient of the functional (3.8) and easily incorporates the constraints (3.9). The fundamental solution (3.2) in the MFS expansion (3.1) is calculated using the MATLAB$^©$ function `besselh`.

3.1. **The plane waves method (PWM).** The plane waves method (PWM) is a meshless Trefftz method closely related to the MFS and applicable to the solution of boundary value problems governed by the Helmholtz or modified Helmholtz equation in simply-connected domains, [2], see also [10, Section 11.1.3]. The PWM removes the parameter η in (3.6), (3.8) and (3.9) but is restricted to the Helmholtz equation whilst the MFS is applicable to any elliptic partial differential equation for which a fundamental solution is explicitly available.

In the PWM we approximate the solution of the problem (2.2), (2.5) and (2.7) by

$$u_N(\boldsymbol{x}) = \sum_{n=1}^{N} C_n \, \mathrm{e}^{\mathrm{i}k\boldsymbol{x}\cdot\boldsymbol{d}_n}, \qquad \boldsymbol{x} \in \overline{D}, \tag{3.11}$$

where the vectors $\boldsymbol{d}_n$ are N distinct unitary direction vectors taken to be

$$\boldsymbol{d}_n = (\cos\phi_n, \sin\phi_n), \quad \phi_n = \frac{2(n-1)\pi}{N}, \quad n = \overline{1, N}, \tag{3.12}$$

and $C_n \in \mathbb{C}$ are unknown complex coefficients to be determined by imposing boundary condition (2.5) and condition (2.7). This results in the minimization of the regularized nonlinear least-squares functional

$$U_{\lambda_1,\lambda_2}(\boldsymbol{C},\boldsymbol{r}) := \sum_{m=1}^{M} \left| \sum_{n=1}^{N} C_n \, \mathrm{e}^{\mathrm{i}k\boldsymbol{x}_m\cdot\boldsymbol{d}_n} + \frac{\mathrm{i}}{4} H_0^{(1)}(k|\boldsymbol{x}_m - \boldsymbol{z}_0|) \right|^2$$

$$+ \sum_{\ell=1}^{L} \left| \sum_{n=1}^{N} C_n \, \mathrm{e}^{\mathrm{i}k\tilde{\boldsymbol{x}}_\ell\cdot\boldsymbol{d}_n} - f^\varepsilon(\tilde{\boldsymbol{x}}_\ell) \right|^2 + \lambda_1 \sum_{j=1}^{N} |C_j|^2 + \lambda_2 \sum_{m=2}^{M} (r_m - r_{m-1})^2, \tag{3.13}$$

subject to the simple bounds on the variables

$$|\boldsymbol{z}_0| < r_m < \zeta_2 = 2.40482/k, \quad m = \overline{1, M}. \tag{3.14}$$

Note that the first two terms in (3.13) impose $2M + 2L$ equations in $M + 2N$ unknowns and we therefore need to take $M + 2L \geq 2N$.

4. NUMERICAL RESULTS AND DISCUSSION

We take, for simplicity, the wave number k equal to unity. In (3.8), we take λ_1 and/or λ_2 equal to zero and base the choice of the non-zero regularization parameter on the L-curve criterion, see [9, 8]. When λ_1 and λ_2 are both non-zero and distinct the L-surface criterion, see [4], might also be employed.

4.1. **Example 1.** We first consider the simple case of a circular scatterer of unit radius. We take $z_0 = (0.5, 0)$ and the measured data on Γ are simulated by solving the direct problem (2.2) and (2.5) using the MFS with $\mathcal{M} = 60$ collocation points, $\mathcal{N} = 40$ singularities on a fixed pseudo-boundary similar to the physical boundary with a magnification factor of $\eta = 1.2$. The data were generated at $L = 32$ points on Γ. In the implementation of the inverse problem we took the initial guess $(c^0, r^0, \eta^0) = (0, 0.6, 1.5)$ and $M = 50$. In Figure 2 we present the reconstructed boundary with no noise and no regularization after $1, 5, 50$ and 200 iterations (`niter`). From this figure it can be seen that there is a very good agreement between the exact and numerical solutions for `niter`=50 and 200. The corresponding results with `niter`=200, noise $p = 5\%$, $\lambda_2 = 0$ and regularization with λ_1, and $\lambda_1 = 0$ and regularization with λ_2, are presented in Figures 3 and 4, respectively. From these figures the following conclusions can be deduced:
– the numerical results without regularization are unstable;
– regularization with λ_1 between 10^{-3} and 10^{-2}, or with λ_2 between 10^{-2} and 10^0 achieves stable and accurate numerical results.
The L-curves corresponding to the two above cases are presented in Figure 5. From Figure 5(a) it may be seen that the corner of the L-curve corresponds to $\lambda_1 = 10^{-3}$ to 10^{-2} which is consistent with the results presented in Figure 3. From Figure 5(b) we observe that the corner of the L-curve corresponds to $\lambda_2 = 1$ which is consistent with the results presented in Figure 4.
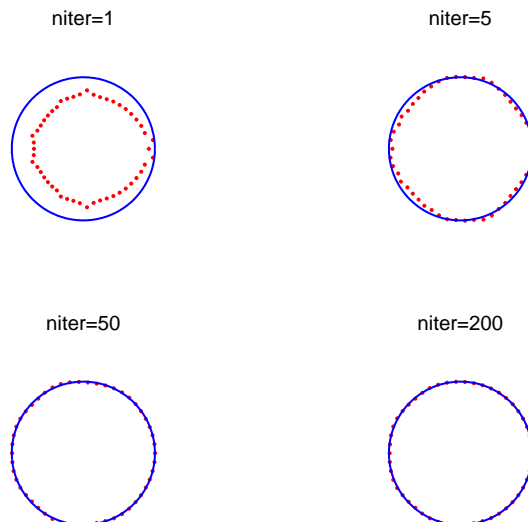

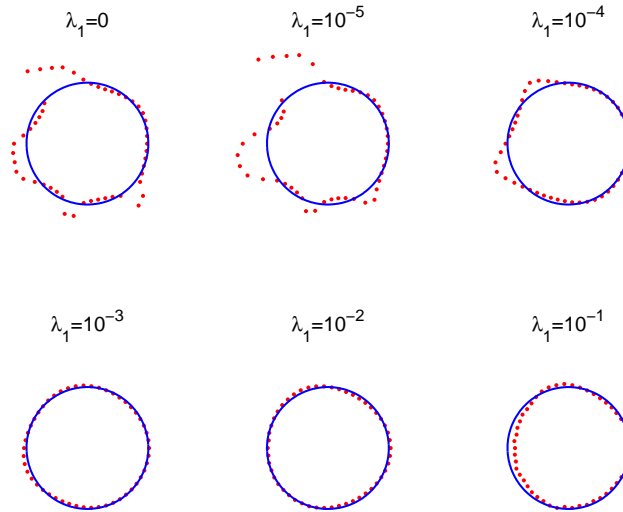FIGURE 2. Example 1: Results for $M = 50, L = 32$, no noise and no regularization for various numbers of iterations.

FIGURE 3. Example 1: Results for $M = 50, L = 32$, noise $p = 5\%$, $\lambda_2 = 0$ and regularization with λ_1.

4.2. **Example 2.** We next consider the case of a peanut shape scatterer given by the radial parametrisation,

$$r(\vartheta) = \frac{1}{2}\sqrt{1 + 3\cos^2\vartheta}, \quad \vartheta \in [0, 2\pi). \tag{4.1}$$

We take $\boldsymbol{z}_0 = (0.25, 0)$ and all the other details are the same as in Example 1. In Figure 6 we present the reconstructed boundary with no noise and no regularization after $5, 10, 50$ and 200 iterations. The corresponding results with `niter`=200, noise $p = 5\%$, $\lambda_2 = 0$ and regularization with λ_1, and $\lambda_1 = 0$ and regularization with λ_2, are presented in Figures 7 and 8, respectively. From these, conclusions similar to those obtained for Example 1 can be drawn.

4.3. **Example 3.** We next consider the case of a complicated scatterer given by the radial parametrisation,

$$r(\vartheta) = 1 + 0.3\cos 3\vartheta, \quad \vartheta \in [0, 2\pi). \tag{4.2}$$

All the details are the same as in Example 2, except for the initial guess which is taken to be $(\boldsymbol{c}^0, \boldsymbol{r}^0, \eta^0) = (\boldsymbol{0}, \boldsymbol{0.4}, \boldsymbol{0}, 1.5)$. In Figure 9 we present the reconstructed boundary with no noise and no regularization after $1, 5, 50$ and 200 iterations. The corresponding results with `niter`=200, noise $p = 5\%$, $\lambda_2 = 0$ and regularization with λ_1, and $\lambda_1 = 0$ and regularization with λ_2, are presented in Figures 10 and 11, respectively. Compared to the previous two examples, the results are less stable and more sensitive to the choice of the regularization parameters λ_1 or λ_2.
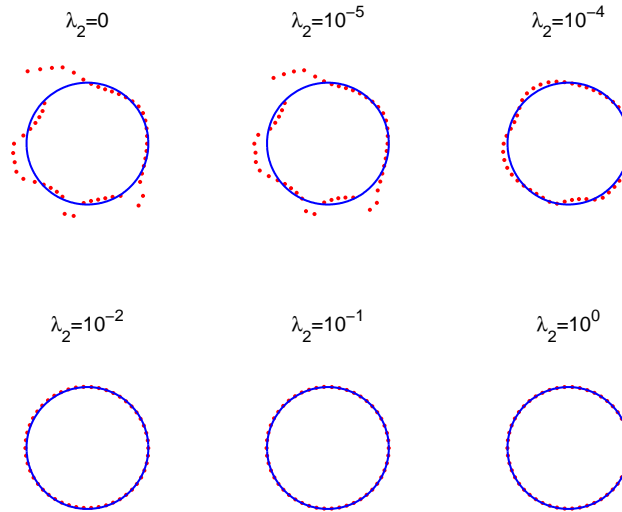
FIGURE 4. Example 1: Results for $M = 50, L = 32$, noise $p = 5\%$, $\lambda_1 = 0$ and regularization with λ_2.

4.4. **Example 4.** We finally consider the case of a scatterer given by the radial parametrisation,

$$r(\vartheta) = 1 + 0.3 \cos 4\vartheta, \quad \vartheta \in [0, 2\pi). \tag{4.3}$$

All the details are taken to be the same as in Example 3. Comparing (4.2) with (4.3) one can see that the scatterer in Example 3 has three petals while the scatterer in Example 4 has four petals. For this more difficult example considerably more iterations were required to obtain an acceptable reconstruction of the scatterer. In Figure 12 we present the reconstructed boundary with no noise and no regularization after $1, 200, 1000$ and 2000 iterations. The corresponding results with `niter`=2000, noise $p = 5\%$, $\lambda_2 = 0$ and regularization with λ_1, and $\lambda_1 = 0$ and regularization with λ_2, were found to be even more sensitive to the choice of λ_1 and λ_2 than for Example 3 and are therefore not presented. Instead, we compare the MFS numerical results of Figure 12 with the numerical results obtained by employing the PWM. In particular, in Figure 13 we present the numerical results obtained using the PWM for Example 4 with the same initial guess, the same values of M and L and $N = 50$. On comparing Figures 12 and 13 it can be seen that the MFS results are considerably more accurate than the PWM results. This conclusion has also been observed for the other Examples 1–3 both with and without noise.

5. CONCLUSIONS

In this paper the MFS was used for the numerical solution of an inverse interior acoustic scattering problem. Since this is an ill-posed problem, its discretized version was regularized with respect to
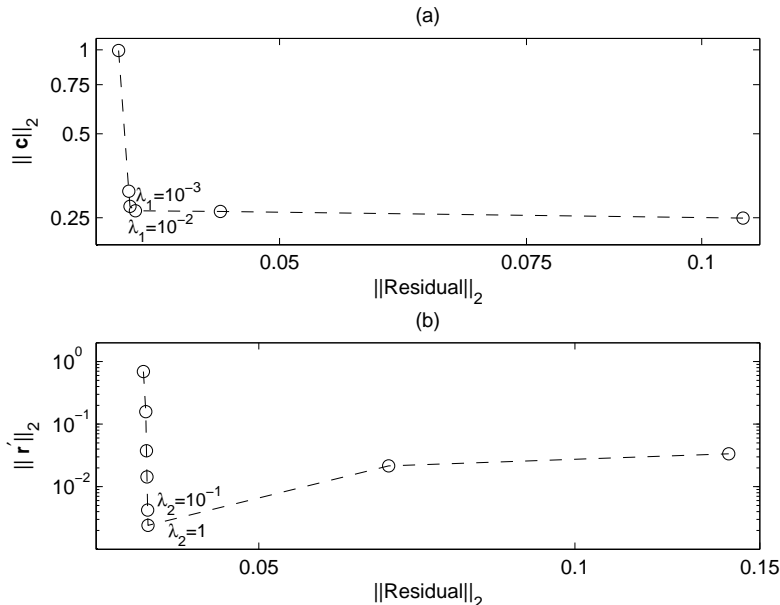
FIGURE 5. Example 1: L-curves for $p = 5\%$. (a) Varying λ_1 with $\lambda_2 = 0$; (a) Varying λ_2 with $\lambda_1 = 0$.

not only the magnitude of the MFS coefficients, but also the smoothness of the curve. The values of the regularization parameters were selected based the L-curve criterion. The numerical results retrieved for four examples revealed that the method is well suited for the reconstruction of the unknown boundaries even when the measured data was contaminated with noise. The analysis was repeated by employing the PWM, but the obtained results were less accurate than the MFS ones. Moreover, comparison with the methods presented in [12, 22, 23] is also satisfactory.

The extension to three dimensions is currently under investigation and involves replacing throughout the function $\dfrac{\mathrm{i}}{4}H_0^{(1)}(k|\boldsymbol{x} - \boldsymbol{z}_0|)$ by $\dfrac{\mathrm{e}^{\mathrm{i}k|\boldsymbol{x}-\boldsymbol{z}_0|}}{4\pi|\boldsymbol{x} - \boldsymbol{z}_0|}$, the constant 2.40482 by π and using spherical coordinates instead of polar coordinates.

The more general and difficult interior inverse scattering problem given by equations (2.2), (2.7) and the boundary condition (2.3) with the impedance boundary operator (2.4d), where λ may or may not be known, [24], is deferred to a future study.

References

[1] C. J. S. Alves and N. F. M. Martins, *The direct method of fundamental solutions and the inverse Kirsch-Kress method for the reconstruction of elastic inclusions or cavities*, J. Integral Equations Appl. **21** (2009), 153–178.

[2] C. J. S. Alves and S. S. Valtchev, *Numerical comparison of two meshfree methods for acoustic wave scattering*, Eng. Anal. Bound. Elem. **29** (2005), 371–382.
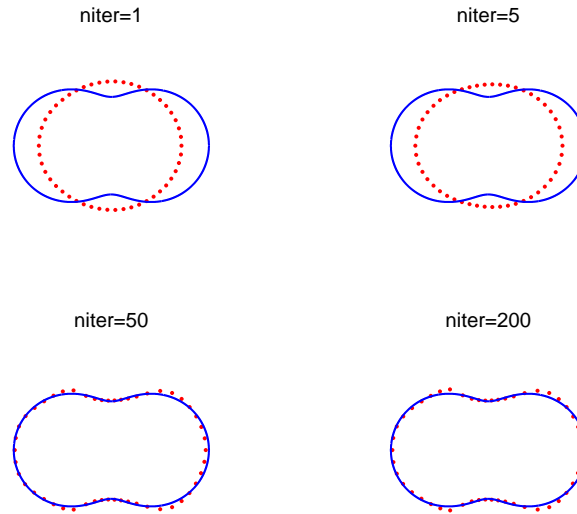
FIGURE 6. Example 2: Results for $M = 50, L = 32$, no noise and no regularization for various numbers of iterations.

[3] C. J. S. Alves, R. Kress and P. Serranho, *Iterative and range test methods for an inverse source problem for acoustic waves*, Inverse Problems **25** (2009), 055005 (17 pp.)

[4] M. Belge, M. E. Kilmer, and E. L. Miller, *Efficient determination of multiple regularization parameters in a generalized L-curve framework*, Inverse Problems **21** (2005), 133–151.

[5] D. Colton and R. Kress, *Inverse Acoustic and Electromagnetic Scattering Theory*, second ed., Applied Mathematical Sciences, vol. 93, Springer-Verlag, Berlin, 1998.

[6] D. Colton and B. D. Sleeman, *Uniqueness theorems for the inverse problem of acoustic scattering*, IMA J. Appl. Math. **31** (1983), 253–259.

[7] G. Fairweather, A. Karageorghis, and P. A. Martin, *The method of fundamental solutions for scattering and radiation problems*, Eng. Anal. Bound. Elem. **27** (2003), 759–769.

[8] P. C. Hansen, *Discrete Inverse Problems: Insight and Algorithms*, SIAM, Philadelphia, 2010.

[9] P. C. Hansen and D. P. O'Leary, *The use of the L-curve in the regularization of discrete ill-posed problems*, SIAM J. Sci. Comput. **14** (1993), 1487–1503.

[10] I. Herrera, *Boundary Methods: An Algebraic Theory*, Applicable Mathematics Series, Pitman (Advanced Publishing Program), Boston, MA, 1984.

[11] O. Ivanyshyn and B. T. Johansson, *A coupled boundary integral equation method for inverse sound-soft scattering*, The 8th International Conference on Mathematical and Numerical Aspects of Waves, Waves 2007, University of Reading, UK, 2007, pp. 153–155.

[12] P. Jakubik and R. Potthast, *Testing the integrity of some cavity - the Cauchy problem and the range test*, Appl. Numer. Math. **58** (2008), 899–914.

[13] B. T. Johansson and B. D. Sleeman, *Reconstruction of an acoustically sound-soft obstacle from one incident field and the far-field pattern*, IMA J. Appl. Math. **72** (2007), 96–112.

[14] A. Karageorghis, D. Lesnic, and L. Marin, *A survey of applications of the MFS to inverse problems*, Inverse Probl. Sci. Eng. **19** (2011), 309–336.
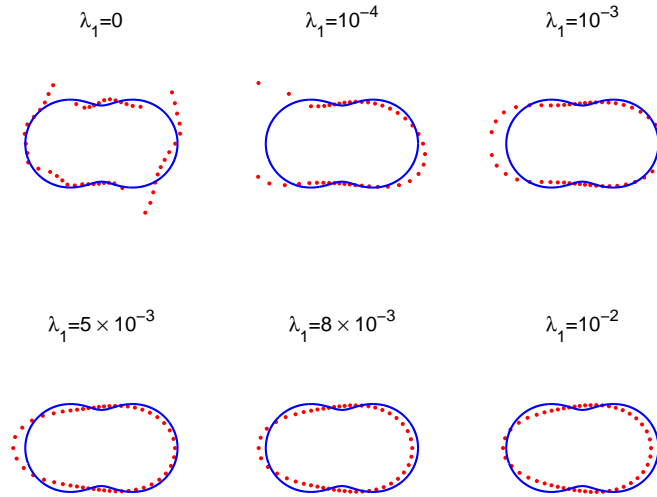
$\lambda_1 = 0$ $\lambda_1 = 10^{-4}$ $\lambda_1 = 10^{-3}$

$\lambda_1 = 5 \times 10^{-3}$ $\lambda_1 = 8 \times 10^{-3}$ $\lambda_1 = 10^{-2}$

FIGURE 7. Example 2: Results for $M = 50, L = 32$, noise $p = 5\%$, $\lambda_2 = 0$ and regularization with λ_1.

[15] A. Karageorghis, D. Lesnic, and L. Marin, *A moving pseudo-boundary MFS for void detection*, Numer. Methods Partial Differential Equations **29** (2013), 935–960.

[16] A. Kirsch and R. Kress, *On an integral equation of the first kind in inverse acoustic scattering*, Int. Ser. Numer. Math. **77** (1986), 93–102.

[17] A. Kirsch and R. Kress, *An optimization method in inverse acoustic scattering*, Boundary Elements IX (C. A. Brebbia, W. L. Wendland, and G. Kuhn, eds.), vol. 3, Springer, Berlin, 1987, pp. 3–18.

[18] P. Kondapalli, D. J. Shippy, and G. G. Fairweather, *Analysis of acoustic scattering in fluids solids by the method of fundamental solutions*, J. Acoust. Soc. Am. **91** (1992), 1844–1854.

[19] R. Kress, *Integral equation method in inverse obstacle scattering*, Eng. Anal. Bound. Elem. **15** (1995), 171–179.

[20] L. Marin and A. Karageorghis, *Regularized MFS-based boundary identification in two-dimensional Helmholtz-type equations*, CMC Comput. Mater. Continua **10** (2009) 259–293.

[21] The MathWorks, Inc., 3 Apple Hill Dr., Natick, MA, *Matlab*.

[22] H.-H. Qin and F. Cakoni, *Nonlinear integral equations for shape reconstruction in the inverse interior scattering problem*, Inverse Problems **27** (2011), 035005 (17 pp).

[23] H.-H. Qin and D. Colton, *The inverse scattering problem for cavities*, Appl. Numer. Math. **62** (2012), 699–708.

[24] H.-H. Qin and D. Colton, *The inverse scattering problem for cavities with impedance boundary condition*, Adv. Comput. Math. **36** (2012), 157–174.

[25] D. J. Shippy, P. S. Kondapalli and G. Fairweather, *Analysis of acoustic scattering in fluids and solids by the method of fundamental solutions*, Math. Comput. Modelling **14** (1990), 74–79.

[26] F. Zeng, P. Suarez and J. Sun, *A decomposition method for an interior scattering problem*, Inverse Probl. Imaging **7** (2013), 291–303.
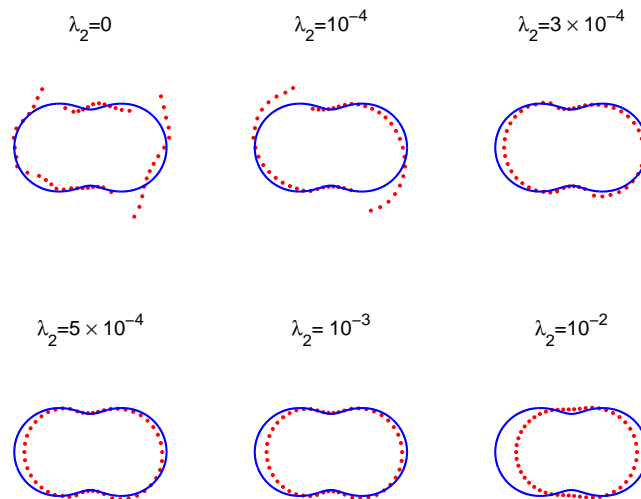
FIGURE 8. Example 2: Results for $M = 50, L = 32$, noise $p = 5\%$, $\lambda_1 = 0$ and regularization with λ_2.

DEPARTMENT OF MATHEMATICS AND STATISTICS, UNIVERSITY OF CYPRUS/ ΠΑΝΕΠΙΣΤΗΜΙΟ ΚΥΠΡΟΥ, P.O.BOX 20537, 1678 NICOSIA/ΛΕΥΚΩΣΙΑ, CYPRUS/ΚΥΠΡΟΣ
E-mail address: `andreask@ucy.ac.cy`

DEPARTMENT OF APPLIED MATHEMATICS, UNIVERSITY OF LEEDS, LEEDS LS2 9JT, UK
E-mail address: `amt5ld@maths.leeds.ac.uk`

DEPARTMENT OF MATHEMATICS, FACULTY OF MATHEMATICS AND COMPUTER SCIENCE, UNIVERSITY OF BUCHAREST, 14 ACADEMIEI, 010014 BUCHAREST, AND INSTITUTE OF SOLID MECHANICS, ROMANIAN ACADEMY, 15 CONSTANTIN MILLE, 010141 BUCHAREST, ROMANIA
E-mail address: `marin.liviu@gmail.com; liviu.marin@fmi.unibuc.ro`
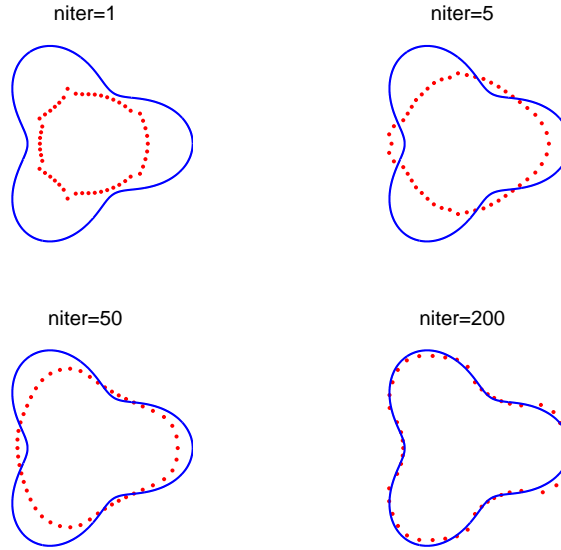
FIGURE 9. Example 3: Results for $M = 50, L = 32$, no noise and no regularization for various numbers of iterations.
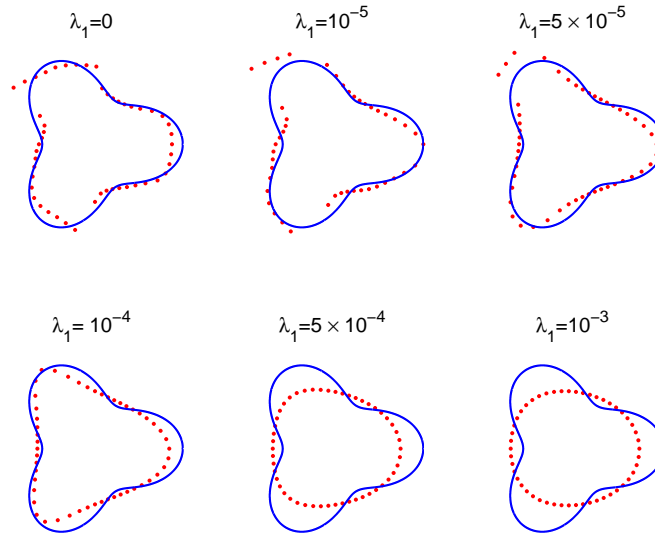

FIGURE 10. Example 3: Results for $M = 50, L = 32$, noise $p = 5\%$, $\lambda_2 = 0$ and regularization with λ_1.
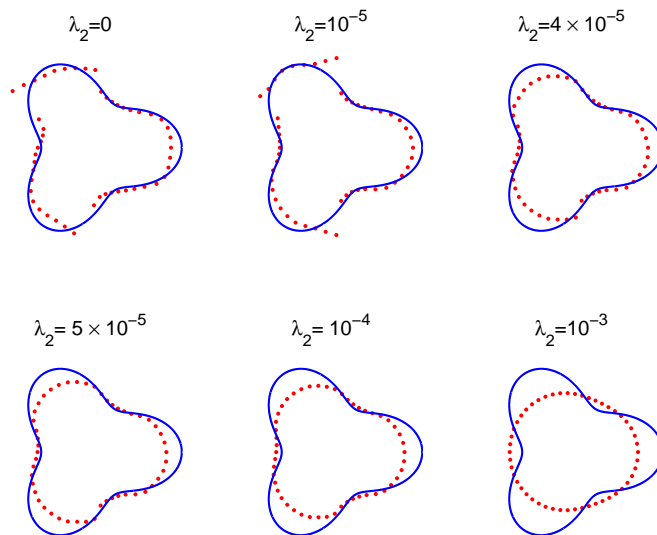
FIGURE 11. Example 3: Results for $M = 50, L = 32$, noise $p = 5\%$, $\lambda_1 = 0$ and regularization with λ_2.
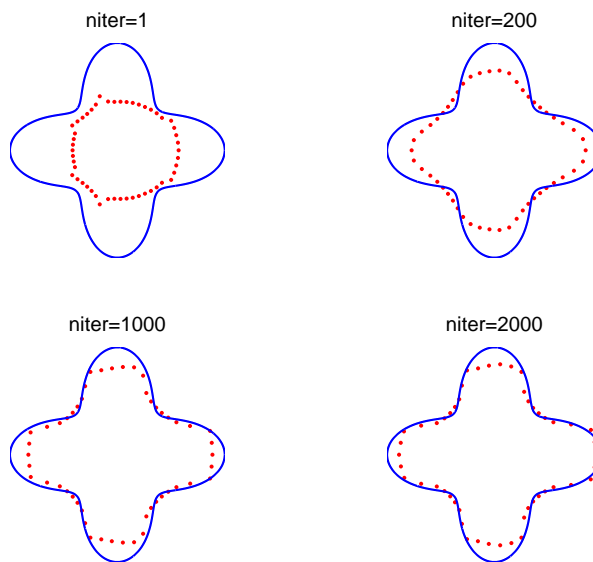

FIGURE 12. Example 4: MFS results for $M = 50, L = 32$, no noise and no regularization for various numbers of iterations.
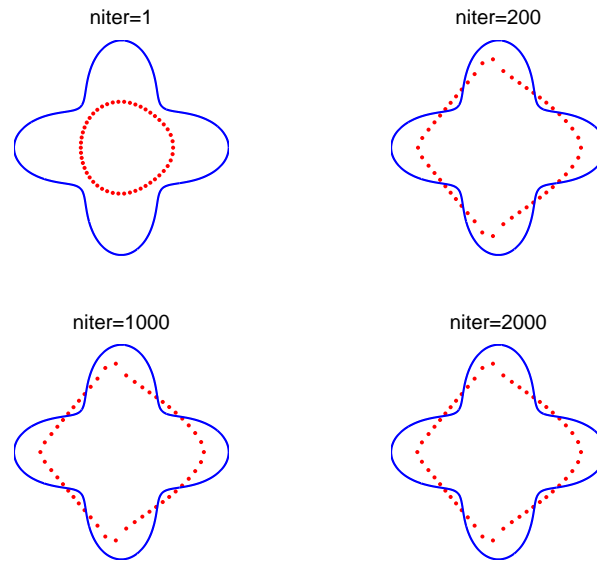
FIGURE 13. Example 4: PWM results for $M = N = 50, L = 32$, no noise and no regularization for various numbers of iterations.